Rapid Communications

$YRuO_3$: A quantum weak ferromagnet

Kunlang Ji,[1] Arpita Paul,[2] Elena Solana-Madruga,[1] Angel M. Arevalo-Lopez,[3] Umesh V. Waghmare,[2] and J. Paul Attfield[1,*]

[1]*Centre for Science at Extreme Conditions and School of Chemistry, University of Edinburgh, United Kingdom*
[2]*Theoretical Science Unit, Jawaharlal Nehru Centre for Advanced Scientific Research, Bangalore 560064, India*
[3]*Université Lille, CNRS, Centrale Lille, ENSCL, Université Artois, UMR 8181–UCCS–Unité de Catalyse et Chimie du Solide, Lille F-59000, France*

(Received 10 June 2020; accepted 2 September 2020; published 21 September 2020)

The perovskite $YRuO_3$ containing low-spin d^5 Ru^{3+} has a *Pnma* orthorhombic structure with elongated RuO_6 octahedra evidencing orbital order and is insulating to low temperatures with a band gap of 70 meV. Canted antiferromagnetic Ru^{3+} spin order is observed below $T_C = 97$ K, and magnetization plateaus that emerge below 62 K reveal a quantum weak ferromagnetic state where 1/8 of the spins are reversed, reflecting extreme single-ion anisotropy resulting from the strong spin-orbit coupling of the d^5 Ru^{3+} ion. Dynamic effects of the reversed spins give rise to an unusual negative AC susceptibility response, and a partial freezing of this motion occurs at 27 K.

DOI: 10.1103/PhysRevMaterials.4.091402

Interesting physics has recently been discovered in materials exhibiting the low-spin electronic configuration of d^5 Ru^{3+} and Ir^{4+} ions, where strong spin-orbit coupling (SOC) leads to an effective $J_{\text{eff}} = 1/2$ quantum ground state [1,2]. The perovskite $SrIrO_3$ is a Pauli paramagnetic metal [3,4] but layered derivatives $Sr_{n+1}Ir_nO_{3n+1}$ ($n = 1$ and 2) are Mott insulators with a gap opened by SOC [5–7]. Spin-spin interactions on honeycomb lattices lead to Kitaev quantum spin-liquid-like behavior, with emergent magnetic Majorana fermions reported in α-$RuCl_3$ [8], and the honeycomb iridate Na_2IrO_3 exhibits the quantum spin Hall effect at room temperature [9]. Ru^{3+} oxides are of interest in this context but are very rare. A series of lanthanide-based $LnRuO_3$ perovskites synthesized at high pressures were found to be Ru-deficient with compositions close to $LnRu_{0.9}O_3$ [10]. The Ln = La, Pr, and Nd materials were found to be semiconducting with no long-range spin order down to 2 K. We have synthesized an essentially stoichiometric sample of $YRuO_3$ [11] and we report here the observation of quantum weak ferromagnetism and an unusual negative AC susceptibility response that demonstrate further new physics arising from the large electronic anisotropy and strong SOC of Ru^{3+}.

Powder x-ray and neutron diffraction analysis [12] show that $YRuO_3$ adopts an orthorhombic *Pnma* tilted perovskite superstructure (lattice parameters $a = 5.824\,80(1)$, $b = 7.554\,15(1)$, and $c = 5.208\ 94(1)$ Å from 300 K synchrotron x-ray refinement). Traces of the pyrochlore phase $Y_2Ru_2O_7$ [13,14] were also observed. Structure refinements using powder neutron data show that the RuO_6 octahedra in $YRuO_3$ are tetragonally elongated with four short (2.04 Å) and two long (2.10 Å) Ru-O bonds. This is consistent with Jahn-Teller distortion and evidences a long-range orbital ordering of t_{2g}^5 Ru^{3+} states as shown in Fig. 1, with the same cooperative Jahn-Teller arrangement as the prototypic orbitally ordered material $LaMnO_3$ [15]. Resistivity measurements show that $YRuO_3$ is insulating down to 30 K with a gap of ~70 meV [11], consistent with the observed orbital ordering, and indicates that $YRuO_3$ is a narrow-band-gap semiconductor with a localized electron ground state, in contrast to the metallicity of the d^5 analog $SrIrO_3$. First-principles density functional calculations confirm that the electron-localized *G*-type antiferromagnetic ground state of $YRuO_3$ is stabilized by on-site electronic correlations of Ru 4*d* electrons, with a Hubbard $U = 4.9$ eV calculated by a self-consistent procedure [16–20]. Electronic isosurfaces reveal the orbital ordering of t_{2g} states [Fig. 1(b)].

DC magnetic susceptibility measurements [Fig. 2(a)] reveal a magnetic transition in $YRuO_3$ at $T_C = 97$ K and a weak magnetic neutron diffraction peak appears on cooling from 100 to 1.7 K [Fig. 2(b)]. This indexes as (½ ½ ½) on a simple perovskite cell showing that *G*-type antiferromagnetic order occurs with each Ru spin coupled antiferromagnetically to six neighbors [21]. The magnetic neutron data are fitted with ordered spins parallel to the *c* axis [Fig. 1(a)], and the refined Ru^{3+} moment is $0.33(3)\,\mu_B$, close to the reported value for α-$RuCl_3$ [22]. Although the apparent spin order is antiferromagnetic, divergence of zero-field and field-cooled susceptibilities reveals that weak ferromagnetism (canted antiferromagnetism) is present. This is observed in many magnetically ordered materials when dominant Heisenberg exchange between spins, represented by the Hamiltonian $-J\boldsymbol{S}_i \cdot \boldsymbol{S}_j$, favors antiferromagnetic order, but a secondary Dzyaloshinskii-Moriya (DM) interaction $-D(\boldsymbol{S}_i \times \boldsymbol{S}_j)$ is allowed by crystal symmetry and leads to a small canting of moments. Weak ferromagnetism is allowed when the ferromagnetic component belongs to the same irreducible symmetry representation as the antiferromagnetic basis, and a coupled loss of inversion symmetry can give rise to a net electric dipole so that weak ferromagnets have been of

*Corresponding author: j.p.attfield@ed.ac.uk

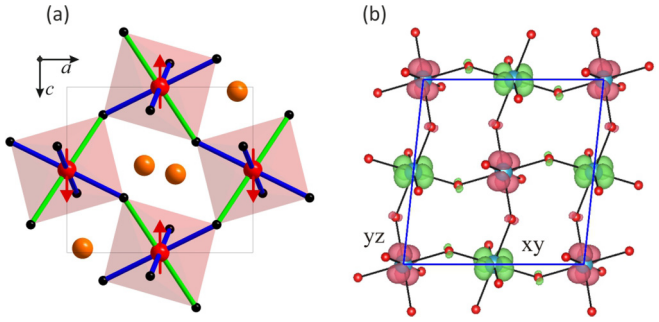

FIG. 1. (a) The *Pnma* unit cell of $YRuO_3$ with Y, Ru, and O depicted in orange, red, and black, respectively. Elongated Ru-O bonds are shown in green and display the cooperative Jahn-Teller distortion arising from orbital ordering. Red arrows show the *G*-type antiferromagnetic structure order of Ru^{3+} moments below 97 K. *a* and *c* axes are shown, and *b* is perpendicular to their plane. (b) Calculated isosurfaces (at 0.02/bohr^3) of magnetization density reveal orbital ordering in $YRuO_3$. The structure is drawn as a $\sqrt{2}\times1\times\sqrt{2}$ supercell of the *Pnma* structure projected on the (010) plane, and shows ordering of Ru d_{xy} (spin-up) and d_{yx} (spin-down) orbitals, colored green and red, respectively. Red and light-blue atoms denote O and Ru.

great interest for type-II multiferroic properties [23]. Magnetic symmetry analysis for $YRuO_3$ reveals that the observed antiferromagnetic order can coexist with a ferromagnetic component parallel to the *b* axis [11]. Similar weak ferromagnetic orders have been reported in other *G*-type *Pnma* perovskites such as $GdFeO_3$ [24–26].

Magnetization-field hysteresis loops in Fig. 3 show that $YRuO_3$ has a weak ferromagnetic moment of $M_w \approx 0.025\,\mu_B$ per ion at low temperatures. Magnetic field cycling of a weak ferromagnet usually results in direct hysteretic switching between the $+M_w$ and $-M_w$ magnetization states and the *M*-*H* loops for $YRuO_3$ have a conventional shape from $T_C = 97$ to 70 K, but between 70 and 60 K magnetization steps emerge at

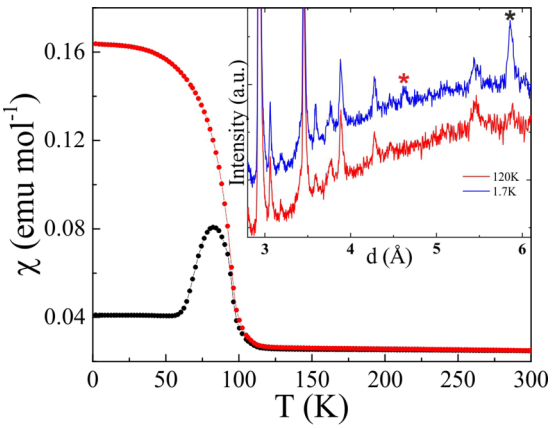

FIG. 2. Zero-field-cooled/field-cooled magnetic susceptibilities (black/red) of $YRuO_3$ under a magnetic field of 0.1 T showing the magnetic ordering transition at $T_C = 97$ K. Inset shows neutron powder diffraction patterns at 1.7 and 120 K. Red star identifies the magnetic peak from spin order in $YRuO_3$; black star marks a spin-ordering peak from the $Y_2Ru_2O_7$ impurity.

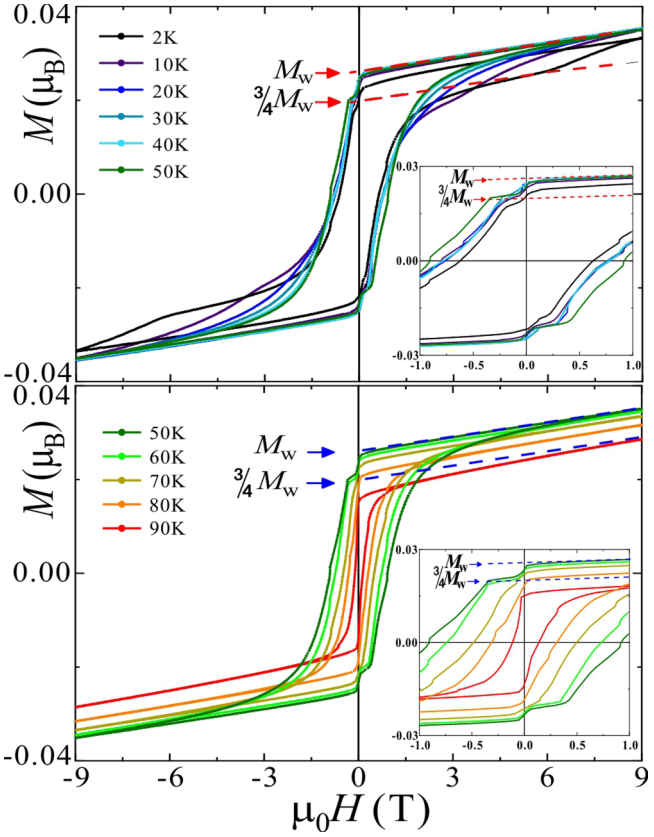

FIG. 3. Magnetization-field hysteresis loops for $YRuO_3$ with loops between 2 and 50 K and between 50 and 90 K separated for clarity. Insets show low-field data. The saturated weak magnetization M_w and the $¾M_w$ quantum weak ferromagnetic features are labeled. M_w is linearly extrapolated from the high-field magnetization to $H = 0$ as shown and the $¾M_w$ line is drawn parallel to the M_w line with $M = ¾M_w$ at $H = 0$.

low fields after field reversal (see lower inset of Fig. 3). The positive magnetization step has magnitude $¾M_w$ and persists to critical field $\mu_0 H_c = -0.35$ T at 50 K. [We describe this as $+¾M_w(-)$ to signify that the magnetization plateau is observed when field is applied in the opposite direction.] On cooling below 30 K, a prominent $+¾M_w(+)$ plateau emerges with increasing field and persists up to a field of 6.2 T at 2 K. Although this switches towards the M_w state at higher fields, it is notable that the maximum field of 9 T is not enough to fully saturate the weak ferromagnetism at 2 K resulting in the apparent small decrease in observed M_w and the $+¾M_w(-)$ plateau.

The observation of a fractional weak magnetization plateau in $YRuO_3$ reveals an unprecedented quantum weak ferromagnetic state that persists to high fields (6.2 T at 2 K). This likely reflects the very high magnetic anisotropy that results from strong SOC in Ru^{3+}. Coercive fields of 52 and 55 T were reported for switching of ferromagnetic orders in Sr_3CoIrO_6 and Sr_3NiIrO_6 reflecting the similarly strong SOC of Ir^{4+} [27]. In such highly anisotropic systems, hysteretic reversal of magnetization by an applied field occurs through 180° flipping of spins so that they remain parallel to their easy axis. A model for the fractional weak ferromagnetism

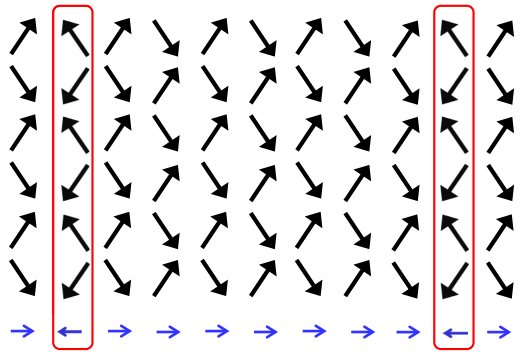

FIG. 4. Model for the ¾M_w quantum weak ferromagnetic state observed in $YRuO_3$. Moments lie parallel to two symmetry-related easy axes resulting from tilting of octahedra. The vertical spin components (parallel to the crystallographic c axis) are coupled antiferromagnetically and weak ferromagnetic (wF) components that arise from DM coupling are ordered in the horizontal (b-axis) direction as shown by the lower blue arrows. The ¾M_w state results from inversion of all moments in every eighth plane, as indicated by the red boxes, so that moments remain parallel to their easy axes while reversing their wF direction.

in $YRuO_3$ in which every eighth plane of moments is reversed, resulting in a long-period spin density wave, is shown in Fig. 4. Octahedral tilting leads to two symmetry-related orbital ordering orientations, as shown in Fig. 1, and these define the local easy axes. In the standard weak ferromagnetic state, the antiferromagnetic spin components are antiparallel to those of all six nearest neighbors with perpendicular weak ferromagnetic (wF) components that arise from DM coupling ordered ferromagnetically. The ¾M_w state requires 1/8 of the wF spin components to be reversed, and results in inversion of the entire moment so that it remains parallel to the easy axis. Further neutron studies will be needed to confirm the spin arrangement in the ¾M_w state.

Quantum magnetic plateau states are reported in many frustrated or low-dimensional spin systems where magnetic field switches order from antiferromagnetic ($M = 0$) in zero field towards saturated ferromagnetic ($M = M_s$) at high field through a series of fractional M/M_s states that emerge at intermediate fields [28,29]. Plateau states correspond to opening of gaps in the magnetic excitation spectrum due to quantum fluctuations which are maximal for $S = ½$ spin ions like Ru^{3+}. Thermally robust plateau states usually have low M/M_s from flipping of a small proportion of spins within the antiferromagnetic phase such as the $M/M_s = 1/3$ state observed in many materials, e.g., CoV_2O_6 [30]. The observation of only a $M/M_w = ¾$ plateau down to 2 K in $YRuO_3$ suggests that a quantum wF state is favored by flipping a small fraction of spins within the full wF order. Further flipping probably leads to avalanche switching directly from +¾$M_w(-)$ to −¾$M_w(-)$ or $-M_w(-)$ states as field decreases, although other fractional wF states may be observable at lower temperatures.

Spin dynamics in $YRuO_3$ at mT field strengths have been investigated by AC susceptibility as shown in Fig. 5. Strong frequency-dependent features are observed between 10 and 60 K and give a negative contribution to the real part of the susceptibility χ' while the large dissipative χ'' imaginary term

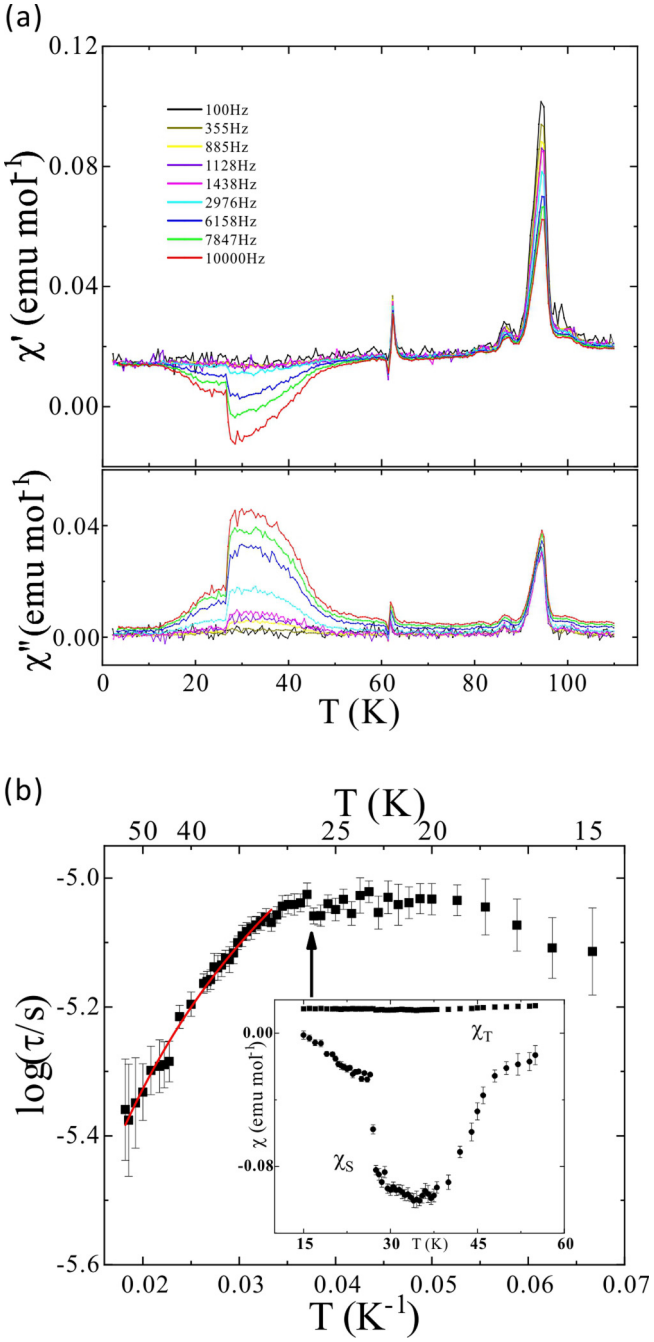

FIG. 5. (a) Real (χ') and imaginary (χ'') parts of the AC susceptibility of $YRuO_3$ measured at frequencies from 100 Hz to 10 kHz between 2 and 110 K with an AC field amplitude of 1.5 mT. The magnetic ordering transition of $YRuO_3$ is seen at 97 K, and a smaller peak at 86 K corresponds to the antiferromagnetic ordering transition of the impurity pyrochlore phase $Y_2Ru_2O_7$ [13,14]. (b) Plot of log(relaxation time) against inverse temperature. The Vogel-Fulcher fit over the 30–55 K range is shown and the vertical arrow marks the 27 K transition in spin dynamics. Inset shows the fitted low- (χ_T) and high- (χ_S) frequency limits of AC susceptibility.

is positive. (This is reminiscent of a superconducting transition although there is no resistive evidence for such behavior in $YRuO_3$.) The anomaly seen at 62 K likely corresponds to the change from the classical (M_w) to the quantum (¾M_w)

weak ferromagnetic state at low fields on cooling, consistent with the emergence of the ¾M_w step between 70 and 60 K in DC hysteresis loops (Fig. 3). The frequency-dependent features show a sharp drop at 27 K and disappear below 10 K. The 27 K discontinuity, below which the prominent +¾M_w(+) plateau emerges in the DC hysteresis loops, has no frequency dependence over the measured 100 Hz to 10 kHz range and so is not a conventional spin-glass transition. Fitting of χ' and χ'' data [31] between 15 and 55 K [11] shows that the limiting low-frequency susceptibility χ_T is positive and essentially constant (Fig. 6 inset), in keeping with the featureless DC magnetization variation in this range [Fig. 2(a)], while the negative contribution and the 27 K transition are seen only in the high-frequency limiting χ_S term that describes the spin dynamics. The average spin-relaxation time τ between 30 and 55 K is found to follow a Vogel-Fulcher temperature dependence $[\tau(T) = \tau_0 \exp(T_a/(T-T_0)]$, which describes dynamic relaxation processes in many inhomogeneous systems such as glasses, relaxor ferroelectrics, and disordered magnets. The fitted parameters are physically plausible as the characteristic time $\tau_0 = 0.15(1)$ ns has a typical magnitude for nonmetallic magnets, $T_0 = 26(1)$ K matches the observed spin dynamics transition at 27 K, and the fitted activation temperature of $T_a = 10.9(1)$ K corresponds to the low-temperature onset of frequency-dependent susceptibility near 10 K in Fig. 5.

The negative χ' response in $YRuO_3$ is highly unusual in insulating magnets (a rare example is a diverging negative χ' in $Na_{0.85}CoO_2$ [32] from Co^{4+} ions with low-spin d^5 configuration like Ru^{3+} in $YRuO_3$) and indicates that the dynamic susceptibility originates from the 1/8 reversed wF spin components within the ¾M_w state, as these are magnetized antiparallel to the bulk magnetization and hence the field direction. Motion of reversed-spin planes (Fig. 4) on field cycling accounts for the large dissipative χ'', and freezing of this motion through pinning to lattice defects is proposed as the origin of the dynamic susceptibility transition observed at 27 K below which the prominent +¾M_w(+) plateau emerges.

In conclusion, $YRuO_3$ perovskite is found to have a *Pnma* orthorhombic structure with elongated RuO_6 octahedra consistent with orbital ordering and a band gap of 70 meV. $YRuO_3$ has a spin-ordered ground state with *G*-type antiferromagnetism observed below $T_C = 97$ K, and magnetization steps that emerge below 62 K evidence an unprecedented quantum weak ferromagnetic state where 1/8 of the spins are reversed, reflecting extreme single-ion anisotropy resulting from the strong spin-orbit coupling of the d^5 Ru^{3+} ion. Dynamical effects of the reversed spins give rise to an unusual negative AC susceptibility response, and a freezing of this motion is proposed as the origin of a spin dynamics transition at 27 K. Fractional weak ferromagnetism is a previously unexplored aspect of the quantum physics of spin-ordered systems, and through magnetodielectric coupling could lead to quantum multiferroic properties.

The authors thank Dr. X. Wang and P. Manual for help with collection of magnetic susceptibility and powder neutron data, respectively. This work was supported by Engineering and Physical Sciences Research Council and Science and Technology Facilities Council.

[1] G. Cao and L. E. DeLong, *Frontiers of 4d- and 5d-Transition Metal Oxides* (World Scientific, Singapore, 2013).
[2] R. D. Cowan, *The Theory of Atomic Structure and Spectra* (University of California Press, Berkeley, 1981).
[3] J. G. Zhao, L. X. Yang, Y. Yu, F. Y. Li, R. C. Yu, Z. Fang, L. C. Chen, and C. Q. Jin, J. Appl. Phys. **103**, 103706 (2008).
[4] P. E. R. Blanchard, E. Reynolds, B. J. Kennedy, J. A. Kimpton, M. Avdeev, and A. A. Belik, Phys. Rev. B **89**, 214106 (2014).
[5] G. Cao, Y. Xin, C. S. Alexander, J. E. Crow, P. Schlottmann, M. K. Crawford, R. L. Harlow, and W. Marshall, Phys. Rev. B **66**, 214412 (2002).
[6] S. J. Moon, H. Jin, K. W. Kim, W. S. Choi, Y. S. Lee, J. Yu, G. Cao, A. Sumi, H. Funakubo, C. Bernhard, and T. W. Noh, Phys. Rev. Lett. **101**, 226402 (2008).
[7] B. J. Kim, Hosub Jin, S. J. Moon, J.-Y. Kim, B.-G. Park, C. S. Leem, Jaejun Yu, T. W. Noh, C. Kim, S.-J. Oh, J.-H. Park, V. Durairaj, G. Cao, and E. Rotenberg, Phys. Rev. Lett. **101**, 076402 (2008).
[8] A. Banerjee, J. Yan, J. Knolle, C. A. Bridges, M. B. Stone, M. D. Lumsden, D. G. Mandrus, D. A. Tennant, R. Moessner, and S. E. Nagler, Science **356**, 1055 (2017).
[9] A. Shitade, H. Katsura, J. Kuneš, X. L. Qi, S. C. Zhang, and N. Nagaosa, Phys. Rev. Lett. **102**, 256403 (2009).
[10] A. Sinclair, J. A. Rodgers, C. V. Topping, M. Misek, R. D. Stewart, W. Kockelmann, J. G. Bos, and J. P. Attfield, Angew. Chem. Int. Ed. **53**, 8343 (2014).
[11] See Supplemental Material at http://link.aps.org/supplemental/10.1103/PhysRevMaterials.4.091402 for further details of sample synthesis, powder diffraction studies and magnetic symmetry analysis, resistivity and magnetization measurements, and electronic structure calculations.
[12] J. Rodriguez-Carvajal, Physica B **192**, 55 (1993).
[13] N. Taira, M. Wakeshima, and Y. Hinatsu, J. Solid State Chem. **144**, 216 (1999).
[14] N. Taira, M. Wakeshima, and Y. Hinatsu, J. Solid State Chem. **152**, 441 (2000).
[15] J. Rodríguez-Carvajal, M. Hennion, F. Moussa, A. H. Moudden, L. Pinsard, and A. Revcolevschi, Phys. Rev. B **57**, R3189 (1998).
[16] P. Giannozzi, S. Baroni, N. Bonini, M. Calandra, R. Car, C. Cavazzoni, D. Ceresoli, G. L. Chiarotti, M. Cococcioni, I. Dabo *et al.*, J. Phys.: Condens. Matter. **21**, 395502 (2009).
[17] J. P. Perdew, K. Burke, and M. Ernzerhof, Phys. Rev. Lett. **77**, 3865 (1996).
[18] G. Kresse and J. Hafner, J. Phys.: Condens. Matter **6**, 8245 (1994).
[19] M. Cococcioni and S. de Gironcoli, Phys. Rev. B **71**, 035105 (2005).
[20] B. Himmetoglu, A. Floris, S. Gironcoli, and M. Cococcioni, Int. J. Quantum Chem. **114**, 14 (2014).
[21] J. Rodriguez-Carvajal, BASIREPS: A Program for Calculating Irreducible Representations of Space Groups and Basis Functions for Axial and Polar Vector Properties (part of the

FULLPROF Suite of programs available at http://www.ill.eu/sites/fullprof, 2007.

[22] A. Banerjee, C. A. Bridges, J. Yan, A. A. Aczel, L. Li, M. B. Stone, G. E. Granroth, M. D. Lumsden, Y. Yiu, J. Knolle, S. Bhattacharjee, D. L. Kovrizhin, R. Moessner, D. A. Tennant, D. G. Mandrus, and S. E. Nagler, Nat. Mater. **15**, 733 (2016).

[23] N. A. Spaldin and R. Ramesh, Nat. Mater. **18**, 203 (2019).

[24] Y. Tokunaga, N. Rurukawa, H. Sakai, Y. Taguchi, T. Arima, and Y. Tokura, Nat. Mater. **8**, 558 (2009).

[25] Z. Y. Zhao, X. M. Wang, C. Fan, W. Tao, X. G. Liu, W. P. Ke, F. B. Zhang, X. Zhao, and X. F. Sun, Phys. Rev. B **83**, 014414 (2011).

[26] X. H. Zhu, X. B. Xiao, X. R. Chen, and B. G. Liu, RSC Adv. **7**, 4054 (2017).

[27] J. Singleton, J. W. Kim, C. V. Topping, A. Hansen, E. D. Mun, S. Chikara, I. Lakis, S. Ghannadzadeh, P. Goddard, X. Luo, Y. S. Oh, S. W. Cheong, and V. S. Zapf, Phys. Rev. B **94**, 224408 (2016).

[28] M. Takigawa and F. Mila, in *Introduction to Frustrated Magnetism. Materials, Experiments, Theory*, edited by C. Lacroix, P. Mendels, and F. Mila, Springer Series in Solid-State Sciences (Springer, Berlin, Heidelberg, 2011), p. 241.

[29] A. Vasiliev, O. Volkova, E. Zvereva, and M. Markina, npj Quantum Mater. **13**, 18 (2018).

[30] M. Markkula, A. M. Arevalo-Lopez, and J. P. Attfield, Phys. Rev. B **86**, 134401 (2012).

[31] M. Balanda, Acta Phys. Pol., A **124**, 964 (2013).

[32] J. S. Rhyee, J. B. Peng, C. T. Lin, and S. M. Lee, Phys. Rev. B **77**, 205108 (2008).